Hindawi
Adsorption Science & Technology
Volume 2023, Article ID 3574652, 14 pages
https://doi.org/10.1155/2023/3574652

Research Article

Study on Phosphorus Adsorption Performance of Inorganic Modified Green Mudstone

Liang Li,[1] **Ke Shi**,[1] **Shaojun Xiong**,[1] **Shimeng Zhang**,[1] **Zhuang Shan**,[1] **Guangsheng Qian**,[2] **Xu Zhai**,[1] **and Ping Xiao**[3]

[1]*Key Laboratory of Ministry of Education on Safe Mining of Deep Metal Mines, Northeastern University, Shenyang 110819, China*
[2]*Department of Civil and Environmental Engineering, Faculty of Science and Technology, University of Macau, Macau 999078, China*
[3]*Fushun Mining Group Co., Ltd, Fushun 113000, China*

Correspondence should be addressed to Liang Li; liliang@mail.neu.edu.cn

Received 22 April 2022; Revised 7 April 2023; Accepted 12 July 2023; Published 1 August 2023

Academic Editor: Selvaraju Narayanasamy

Inorganic modified green mudstone (MGM) was prepared from the green mudstone (GM) residue of Fushun West Open Pit Mine and characterized by XRF, XRD, FTIR, and SEM of GM and MGM. According to the calculation of pore size and the BET equation, the pore size and specific surface area of the MGM were larger. The results of adsorption kinetics and isothermal adsorption experiments showed that the adsorption capacity of MGM for phosphate increased from 0.1 mg/g to 0.71 mg/g, which was obviously better than that of GM. The GM and MGM accorded with the quasi-second-order kinetic model. The isothermal adsorption data of GM accorded with the Freundlich model, and the isothermal data of MGM accorded with the Langmuir model, which indicated that the model of GM and MGM was an adsorption process from a double layer to a single layer. Thermodynamic data showed that the increase in temperature was beneficial to the adsorption of MGM. The internal diffusion model showed that due to the change of pore size structure after modification, the number of adsorption sites that could provide phosphate was increased, and at the same time, the change of internal elements led to the extension of the chemical reaction time by 700 min. Because of the ligand exchange and electrostatic interaction between phosphate, GM, and MGM, the adsorption results showed that acidity was better than alkalinity. To improve the recycling ability of MGM, hydrochloric acid with a concentration of 0.1 mol/L was determined as the best phosphorus resolving agent, and the resolving rate was still close to 80% after five cycles. The results showed that the MGM could be a promising adsorbent for the removal of phosphorus, providing a new way for resource utilization of mining waste residue.

1. Introduction

With the continuous development of society, increasing eutrophic substances such as nitrogen and phosphorus have been produced and discharged by human production activities [1], and the excessive amount of phosphorus introduced into the water leads to eutrophication. Eutrophication of the water body reduces the content of dissolved oxygen in the water body, making a large number of plants and fish unable to live [2], and at the same time, it also affects the self-purification ability of the water body. Phosphorus is considered to be the limiting nutrient that affects the eutrophication of lakes [3, 4], and when the total phosphorus concentration in water exceeds 0.02 mg/L, algal blooms may occur [5]. From this point of view, strict controlling of the phosphorus content in water bodies is very important to prevent eutrophication [6]. With the rapid economic development, the extensive use of phosphorus-containing products, and the limited advanced wastewater treatment technology, the phosphorus content is increasing at an alarming rate [7, 8]. Therefore, it is essential to develop an efficient and economical phosphorus removal method.

Nowadays, affected by the global population growth and water shortage, more and more methods are applied to the treatment of phosphorus-containing wastewater, including

chemical methods [9], biological methods [10], and adsorption methods [11]. Removal of chemical phosphorus removal requires a large amount of chemical reagents, and a large amount of chemical sludge is produced, which is not easy to clean and can easily cause secondary pollution, limiting its popularity [12]. Biological phosphorus removal depends on organic load [13], water temperature, and other parameters [14], which leads to a decrease in stability and reliability. However, comparing the above methods, we can see that the adsorption method has the advantages of easy operation and maintenance, high removal efficiency, low-cost, and low-energy consumptions [15]. At present, the phosphorus adsorbents studied and applied mainly include natural materials, industrial waste residue, and synthetic adsorbents [16]. However, the adsorption efficiency of natural materials is generally low, while synthetic adsorbents have some disadvantages, such as high price and complex synthesis methods. Based on the consideration of high efficiency, economy, and environment, industrial wastes are used as phosphorus removal adsorbents, such as copper tailings [17] and fly ash [18]. The research showed that it was advisable to use waste as resources, but many materials have insufficient adsorption and regeneration capacity, poor selectivity, and limited surface area [19]. Therefore, many modification methods, such as heat modification [20], inorganic modification [21], or organic modification [22], have been used to improve the adsorption capacity.

Fushun West Open Pit Mine was once the largest open-pit coal mine in Asia. It has a history of 100 years, producing 1 billion tons of coal in total. Now, it has formed a deep pit with a length of 6.6 km from east to west, a width of 2.2 km from north to south, and a depth of more than 400 m, with a disturbed area of more than 15 km^2. The waste residue produced in the mining process includes oil shale waste residue, coal gangue, and green mudstone (GM), which seriously harms the atmosphere, land, and water environment in the mining area. The Fushun West Open Pit Mine is going to be shut down. After the pit is closed, the surrounding surface water and groundwater will gradually seep into the pit, and the agricultural nonpoint source pollutants around the pit will also probably enter the pit. Blocking agricultural nonpoint source sewage containing phosphorus from entering the pit to avoid water eutrophication is one of the difficult problems to be solved. GM belongs to clay mineral and has a good adsorption effect on uranium [23]. However, there is no report regarding the adsorption of phosphate by GM. Therefore, it is the first time to attend to prepare GM of pit waste into a material with good adsorption capacity for phosphorus removal so as to prevent and control the pollution of agricultural nonpoint source sewage.

The study was designed to investigate the performance of GM and inorganic modified green mudstone (MGM) on phosphate adsorption. The apparent structure, kinetic, equilibrium isotherm, thermodynamic, and adsorption stability experiments of GM and MGM were studied. In addition, the mechanism of MGM adsorption was attempted to be demonstrated. This provides not only a new way for the resource utilization of pit waste but also provides a new material for the removal of phosphorus in wastewater, so as to achieve the purpose of treating waste with waste.

2. Materials and Methods

2.1. Materials. The GM was collected from the GM dump on the east side of the Fushun West Open Pit Mine in April 2019 (longitude between 123.9134 and 123.9081, latitude between 41.8439 and 41.8485). Potassium dihydrogen phosphate (KH_2PO_4), sodium hydroxide (NaOH), hydrochloric acid (HCl), aluminum sulfate ($Al_2(SO_4)_3$), and magnesium chloride ($MgCl_2$) were obtained from Sinopharm Chemical Reagents Co., Ltd.

The XRD of GM is shown in Figure 1. The XRD pattern was analyzed according to the study [24]. According to the analysis of the XRD spectrum, the main components of GM are muscovite ($KAl_2((AlSi_3)O_{10})(OH)_2$, 2θ: 8.891, 20.02, 30.025, and 35.242), potassium feldspar ($K(AlSi_3O_8)$, 2θ: 25.56, 26.42, 27.08, and 27.46), montmorillonite ($Ca_2(Al_{0.93}Fe_{0.05})$ $Al(Al_{0.24}Fe_{0.76})Si_3O_{13}H$, 2θ: 7.423, 19.625, 26.426, and 34.331), and analcime ($Na(AlSi_2O_6)(H_2O)$, 2θ: 15.78, 25.96, and 30.51).

2.2. Material Preparation

2.2.1. Preparation of GM. The GM sample was a mixture of four samples. After being crushed, the GM was sieved with a 100-mesh sieve and then washed with deionized water with a magnetic stirrer 3 times, each time for 10 min. After washing, the GM was put into an oven to dry for subsequent experiments.

2.2.2. Preparation of MGM. 10 g of GM was mixed with 100 mL of a 1.0 mol/L NaCl solution, and then the mixture solution was stirred at 293 K for 20 h. Next, the solid product was separated by centrifugation and, subsequently, it was mixed with 100 mL of 1.0 mol/L NaCl solution, and then the mixture solution was shaken at 293 K for 20 h. Next, the solid product was separated by centrifugation and washed with distilled water. After drying at 102°C, sodium-type GM was prepared. Sodium-type GM, aluminum sulfate, and magnesium chloride were mixed with water in a mass ratio of 8 : 2 : 1, and a 1.0 mol/L NaOH solution was added dropwise to the mixture until the pH value reached 7.0. Then, the mixture was heated and dried in an oven for 48 h at a temperature of 375 K, then heated in a muffle furnace for 10 h at a temperature of 673 K, naturally cooled, sieved with a 100-mesh sieve, and stored in a sealed bag for subsequent use.

2.3. Adsorption Experiments

2.3.1. Adsorption Kinetic Experiment. The kinetic adsorption experiment of phosphorus in wastewater by GM and MGM was studied. 4 g of GM and MGM were, respectively, mixed with 100 mL of 5 mg/L KH_2PO_4 (calculated as *P*) solution, and a 1.0 mol/L NaOH solution was added dropwise to the mixture until the pH value reached 7.0. Then the mixture solution was mixed at 298 K and 150 r/min for different times (10, 20, 30, 40, 60, 240, 480, 720, 1440, 2160, and 2880 min). The sample was filtered by 0.45 μm membrane, and then the concentration of phosphorus in the filtrate was determined by a UV-vis spectrophotometer (3 parallel experiments were done for each concentration).

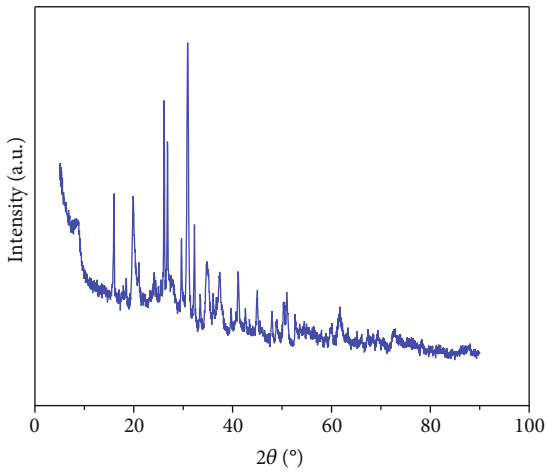

Figure 1: The mineral composition of GM.

The amount of phosphate adsorbed onto the samples at different time periods (q_e) was calculated by the following equation:

$$q_e = \frac{(C_0 - C_e)V}{m}, \quad (1)$$

where q_e represented the adsorption amount of phosphorus at equilibrium (mg/g); C_0 and C_e were the initial concentration of phosphorus and the concentration at equilibrium (mg/L); V was the solution volume (L); and m was the content of GM and MGM (g).

The adsorption kinetic model of GM and MGM for phosphorus was analyzed by the quasi-first-order kinetic model (Formula (2)), quasi-second-order kinetic model (Formula (3)), and intraparticle diffusion model (Formula (4)) [25, 26].

$$\ln (q_e - q) = \ln q_e - k_1 t, \quad (2)$$

$$\frac{t}{q} = \frac{1}{k_2 q_e^2} + \frac{t}{q_e}, \quad (3)$$

$$q_t = k_3 t^{1/2} + C, \quad (4)$$

where t was the reaction time (h); q_t was the adsorption capacity of GM and MGM on phosphorus (mg/g) at different times; and k_1, k_2, and k_3 were the rate constants of the quasi-first-order kinetic model, quasi-second-order kinetic model, and intra-particle diffusion model, respectively.

2.3.2. Adsorption Isothermal Experiment. The isothermal adsorption experiments of phosphorus in wastewater by GM and MGM at 293 K and 303 K were studied. 4 g of GM and MGM were, respectively, mixed with 100 mL KH_2PO_4 (calculated as P) solutions with different concentrations (0, 1, 2, 3, 5, 8, 10, and 15 mg/L), and a 1.0 mol/L NaOH solution was added dropwise to the mixture until the pH value reached 7.0. Then, the mixture solution reacted for 24 h under the condition of shaking table rotation speed of 150 r/min for sampling. The sample was filtered by 0.45 μm membrane, and then the concentration of phosphorus in the filtrate was determined by a UV-vis spectrophotometer (3 parallel experiments were done for each concentration).

Table 1: Chemical composition of GM and MGM.

Parameter	GM (%)	MGM (%)
SO_2	42.94	42.96
Al_2O_3	15.52	16.61
TFeO	12.86	12.10
CaO	12.53	4.51
MgO	3.56	4.85
TiO_2	1.28	0.96

According to the change of average phosphorus concentration infiltrate, the isothermal adsorption parameters of GM and MGM on phosphorus were analyzed. The Langmuir (Formula (5)), Freundlich (Formula (6)), and Temkin (Formula (7)) were used to fit all experimental results [27–29].

$$\frac{C_e}{q_e} = \frac{1}{q_m K_L} + \frac{C_e}{q_m}, \quad (5)$$

$$\ln q_e = \ln K_F + \frac{1}{n} \ln C_e, \quad (6)$$

$$q_e = A + B \ln C_e, \quad (7)$$

where C_e was the concentration of phosphorus in the filtrate after adsorption equilibrium (mg/L); q_e was the adsorption amount of GM and MGM to phosphorus after adsorption equilibrium (mg/g); q_m was the maximum adsorption amount of GM and MGM to phosphorus (mg/g); and K_L, K_F, and B were adsorption equilibrium constants.

2.3.3. Adsorption Thermodynamic Experiment. Thermodynamic research included the study of ΔG, ΔH, and ΔS in the adsorption process, so that we could find out whether the adsorption process occurs spontaneously and analyze the forces driving the adsorption. Thermodynamic parameters calculated by formula (8) [30]

$$\begin{gathered} \Delta G = -RT \ln K, \\ \ln \left[\frac{K_{T2}}{K_{T1}}\right] = -\frac{\Delta H}{R}\left[\frac{1}{T_2} - \frac{1}{T_1}\right], \\ \Delta G = \Delta H - T\Delta S, \end{gathered} \quad (8)$$

where R was the gas constant, with a value of 8.134 J/(molK), and T was the Kelvin temperature (t). The ln K value was the straight line intercept obtained by plotting ln (Q_e/C_e) against Q_e. When $\Delta G < 0$, the adsorption process was spontaneous. On the contrary, it was involuntary. When $\Delta H < 0$, the adsorption process was exothermic; on the contrary, it was endothermic. When $\Delta S < 0$, it indicated that the chaos of the system decreased; on the contrary, the system was more disorderly.

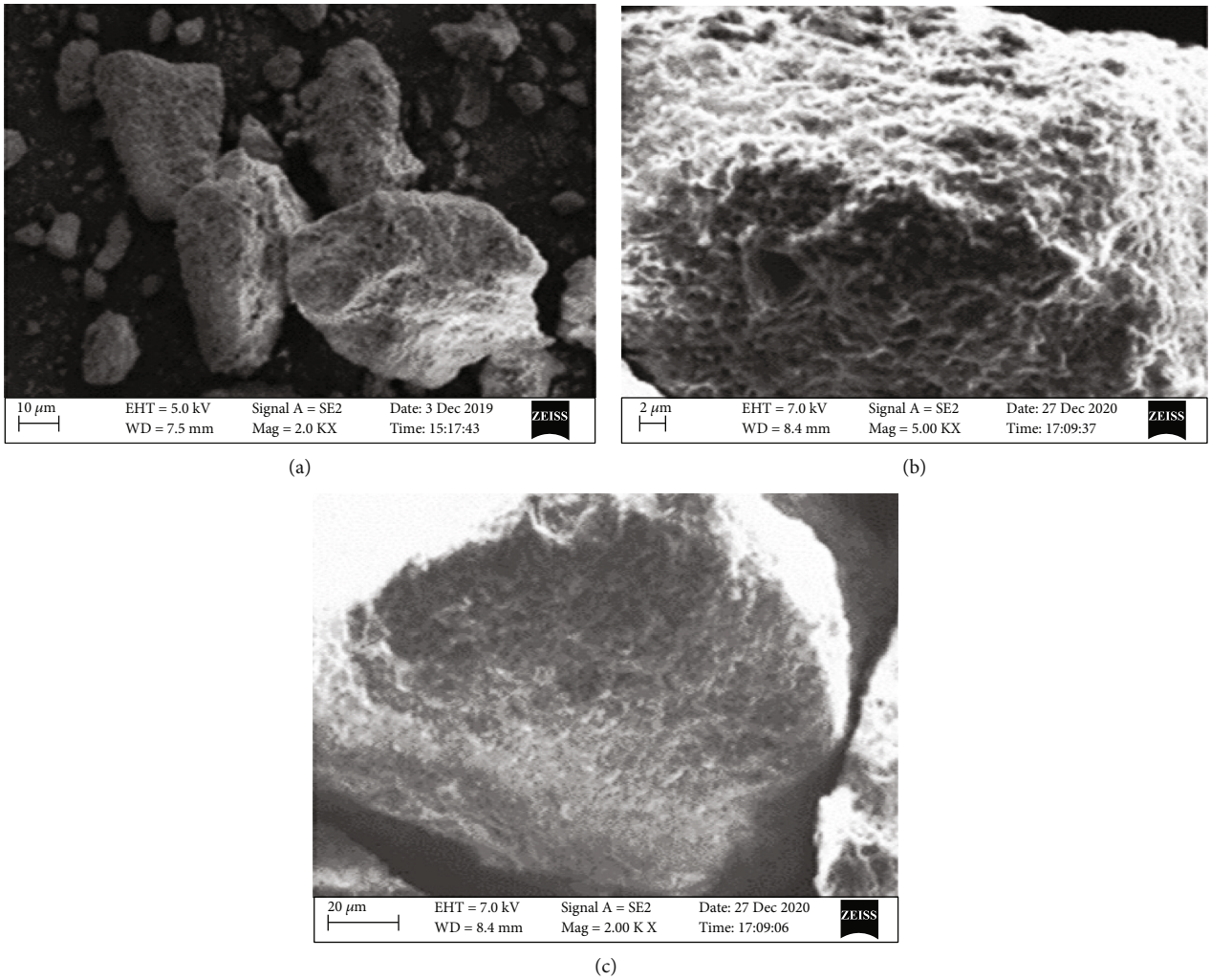

Figure 2: SEM of GM before (a) and after (b) modification and before (a, b) and after (c) adsorption.

2.3.4. Adsorption Stability Experiment

(1) The pH Adaptability of Adsorbent. The effects of pH values of 5, 7, and 9 on the adsorption of phosphorus in wastewater by GM and MGM were studied. HCl or NaOH were used to adjust the pH of the solution. 4 g GM and MGM were mixed with 100 mL of 5 mg/L KH_2PO_4 (calculated as *P*) solution and agitated at 150 rpm in a temperature-controlled shaker at 298 K for 24 h.

(2) Recycle Stability of Adsorbent. After the adsorption experiment, the phosphorus solution in the conical flask was poured out, and then the MGM after the adsorption reaction was washed twice with deionized water. 4 g of MGM after the adsorption reaction was mixed with hydrochloric acid and sodium hydroxide solution with a concentration of 1 mol/L, respectively. After shaking at a constant temperature of 298 K and 150 r/min for 24 h, samples were taken for the adsorption experiment. Five adsorption regeneration experiments were carried out.

2.4. Analysis Methods and Characterization. TP were determined by the national standard method. A scanning electron microscope (SEM) (SIGMA 300) was used to measure the structure and morphology of GM and MGM. X-ray fluorescence spectroscopy (XRF, ZSX primus, Rigaku, Japan) was used to analyze the main chemical components of GM and MGM. The mineral composition of GM was analyzed by X-ray diffractometer (XRD, PANalytical X'Pert PRO, PANalytical, Netherlands). Fourier-transform infrared spectroscopy (FT-IR, iS10, Thermo Fisher, USA) was used to study the functional groups on the surfaces of GM and MGM samples. The BET method was used to calculate the specific surface area of GM and MGM, and BJH theory was used to calculate the pore volume and pore size distribution of GM and MGM. The pH value of the solution was measured using a pH meter (PB-10 Sartorius).

3. Results and Analysis

3.1. Characterization

3.1.1. XRF Analysis of GM and MGM. The XRF analysis results of GM and MGM are shown in Table 1.

It could be seen from Table 1 that the content of SO_2 and TFeO in the MGM had little change. While the content of Al_2O_3 and MgO increased by 1.09% and 1.29%, respectively, and the content of CaO reduced from 12.53% to 4.51%, which was the result of the cation exchange of Al^{3+}, Mg^{2+}, and Na^+ with Ca^{2+}. However, the generated $CaCl_2$ volatilized in the subsequent calcination process, resulting in mass loss and Ca^{2+} reduction.

3.1.2. SEM Analysis of GM and MGM. The SEM results of GM, MGM, and adsorption are presented in Figure 2. As shown in Figures 2(a) and 2(b), the micropores of the GM were more obvious. This showed that the MGM had a higher porosity and proved that the MGM had better adsorption capacity. As shown in Figures 2(b) and 2(c), the surface of the adsorbed MGM was smooth because its surface was filled with adsorbed sulfate ions. So, the modified porosity was beneficial for the diffusion of pollutants in micropores. Furthermore, the surface roughness of the MGM was greater. This structure not only enhanced the electrostatic force but also absorbed more phosphate ions. Therefore, the adsorption characteristics of MGM were more obvious.

3.1.3. FTIR Analysis of GM and MGM. The FTIR spectra of GM and MGM samples in the wave number range of 4000-500 cm^{-1} are shown in Figure 3. The spectra of GM and MGM were obviously different at 1440 cm^{-1}, and this absorption peak was C-H bending [24]. The absorption peaks of hydroxyl (O-H) at 3615 and 3669 cm^{-1} were O-H stretching vibration [31], which indicated that both GM and MGM contained hydroxyl groups [32]. The bending vibration of -OH at 1633 cm^{-1} was mainly related to the absorbed water inside the sample [33]. GM was composed of a Si-O tetrahedron. After being activated and modified by Al^{3+} and Mg^{2+}, the increased Al^{3+} replaced the position of Si^{4+} in the silicon-oxygen tetrahedron of GM, so the absorption peak intensity of 1033 cm^{-1} changes before and after modification.

3.1.4. Specific Surface Area and Pore Size Structure of GM and MGM. The shape, number, and size of the pores had a close relationship with the performance of adsorbents. According to international regulations, pores with a pore size less than 2 nm were called micropores; pore sizes between 2 and 50 nm were called mesopore; and apertures larger than 50 nm were called macropores [34]. The pore size distribution of GM and MGM is shown in Figure 4. It could be seen from Figure 4 that the pore size of GM and MGM was between 2 and 40 nm, which was mesopore. The difference was that the MGM pore size ranged from 3 nm to 38 nm and was concentrated at 7 nm, and the average pore size changed from 5.258 nm to 7.065 nm, increasing by 1.807 nm. The maximum pore size was increased from 35 nm to 38 nm, and the pore size was clearly increased. In this experiment, the BET equation was used to calculate the specific surface area of the MGM from 46.58 m^2/g to 52.66 m^2/g. The pore volume changed from 0.074 cm^3/g to 0.096 cm^3/g, increasing by 0.022 cm^3/g. Studies have shown that increasing the specific surface area and pore volume

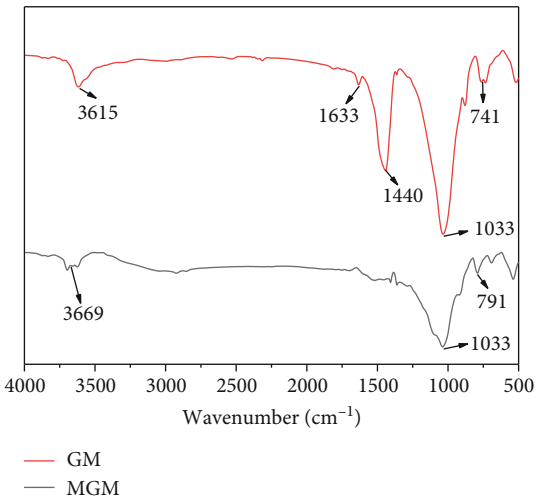

Figure 3: FT-IR spectra of GM and MGM.

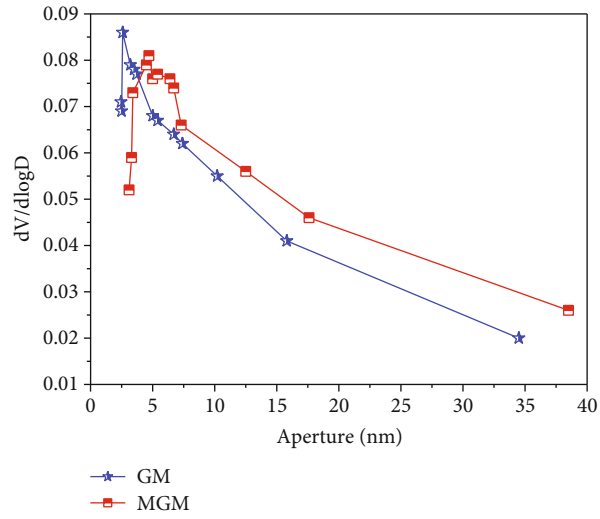

Figure 4: Pore size distribution diagram.

provided more active sites, thus improving the adsorption capacity of minerals to phosphorus [35].

The adsorption-desorption isotherm diagram of GM and MGM is shown in Figure 5. It could be seen from Figure 5 that the adsorption-desorption curves of GM and MGM were all type IV. The hysteresis ring could also be used as one of the bases to judge the width of the pore size distribution. The existence of hysteresis ring indicated the existence of mesoporous structure [36]. A hysteresis ring was produced when P/P_0 was 0.45-1.00. The closed endpoint of the hysteresis ring reflected the width of the pore size. It could be obtained from this that the hysteresis loops of GM and MGM were all mesopores, and the hysteresis loops did not rise sharply when P/P_0 was 1.0 closed, indicating that there were fewer macropores in GM and MGM, and mesopores were the main ones. Figure 5 also shows that the adsorption capacity of MGM increased. Therefore, the comparison of adsorption-desorption isotherms, specific surface area, and pore size of GM and MGM confirmed

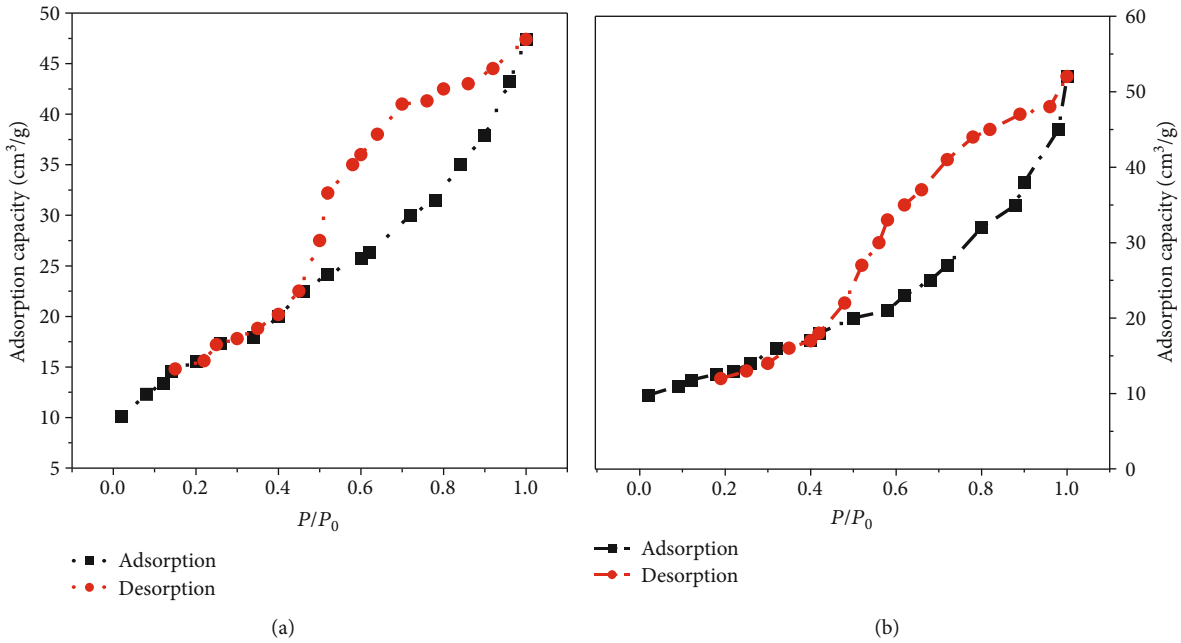

Figure 5: Adsorption and desorption isotherms of GM (a) and MGM (b).

the conclusion of SEM, and it was concluded that one of the reasons for the increase in the adsorption capacity of MGM was related to its surface structure.

3.2. Dynamics Research

3.2.1. Quasi-Primary and Quasi-Secondary Models. Quasi-first-order and quasi-second-order kinetic equations were used to fit the experimental data of phosphorus adsorption onto GM and MGM. The fitting curve is shown in Figures 6(a)–6(d). The fitting results are shown in Table 2. It could be seen from Table 2 that the R_{2^2} values in GM and MGM were both 0.999. This showed that both of them followed the quasi-second-order kinetic equation. Kinetics was used to evaluate the reaction time and the maximum adsorption capacity [37]. The adsorption kinetic curves of GM and MGM are shown in Figure 6(e). It could be concluded from Figure 6(e) that the adsorption rate of the adsorbent was consistent with the rapid increase in the initial reaction time and then slowly increased to ensure the precipitation of phosphorus, consistent with the known research trends [38]. The maximum q_e of GM and MGM was increased from 0.1 mg/g to 0.71 mg/g, and the time to reach adsorption equilibrium was pushed back by approximately 700 min.

3.2.2. Particle Internal Diffusion Model. In order to further study the adsorption process of phosphorus by GM and MGM, the intraparticle diffusion model was studied. The fitting results are shown in Table 2. It could be seen from Figure 6(f) that the whole adsorption process of GM and MGM could be divided into three stages. In the first stage, the slope of the straight line was the largest, indicating that the adsorption rate was the fastest. The reason may be that a large number of phosphate ions are rapidly attached to the surface of GM due to electrostatic action. As phosphate ions slowly filled the surface of GM, the boundary layer resistance became larger and larger, leading to the gradual decline of the adsorption rate, so the slope became slower. At this time, the adsorption process changed from electrostatic adsorption to chemical adsorption. This was because there were a large number of pore structures on the surface of GM. At the beginning of adsorption, because of electrostatic attraction, a large number of phosphate ions quickly entered into the pores of the GM, resulting in an increase in the adsorption capacity. In the second stage, the surface pore size of GM was basically occupied by phosphate ions and reached saturation, and the adsorption mode was changed to chemical adsorption. In the third stage, the reaction was gradually completed and equilibrium was reached. The difference between GM and MGM was that the phosphate groups in the pore size structure of the MGM in the first stage were clearly greater than those of the GM, and the chemical reaction time in the second stage was also longer than that of the GM. With the addition of the two, the whole adsorption process was delayed by 700 min compared with that of GM. The reason for this phenomenon may be that the change in the pore structure after modification can provide more adsorption sites for phosphate, and the change in the internal elements leads to the extension of the chemical reaction time.

3.3. Adsorption Isotherm. The adsorption characteristics of GM and MGM of phosphate solutions with different concentrations were studied at 293 K and 303 K. The Langmuir, Freundlich, and Temkin equation data fitting at different temperatures are shown in Tables 3 and 4.

It could be seen from Table 3 that the adsorption process of phosphate by GM at 293 K and 303 K accorded with the Freundlich adsorption model. Because Freundlich described

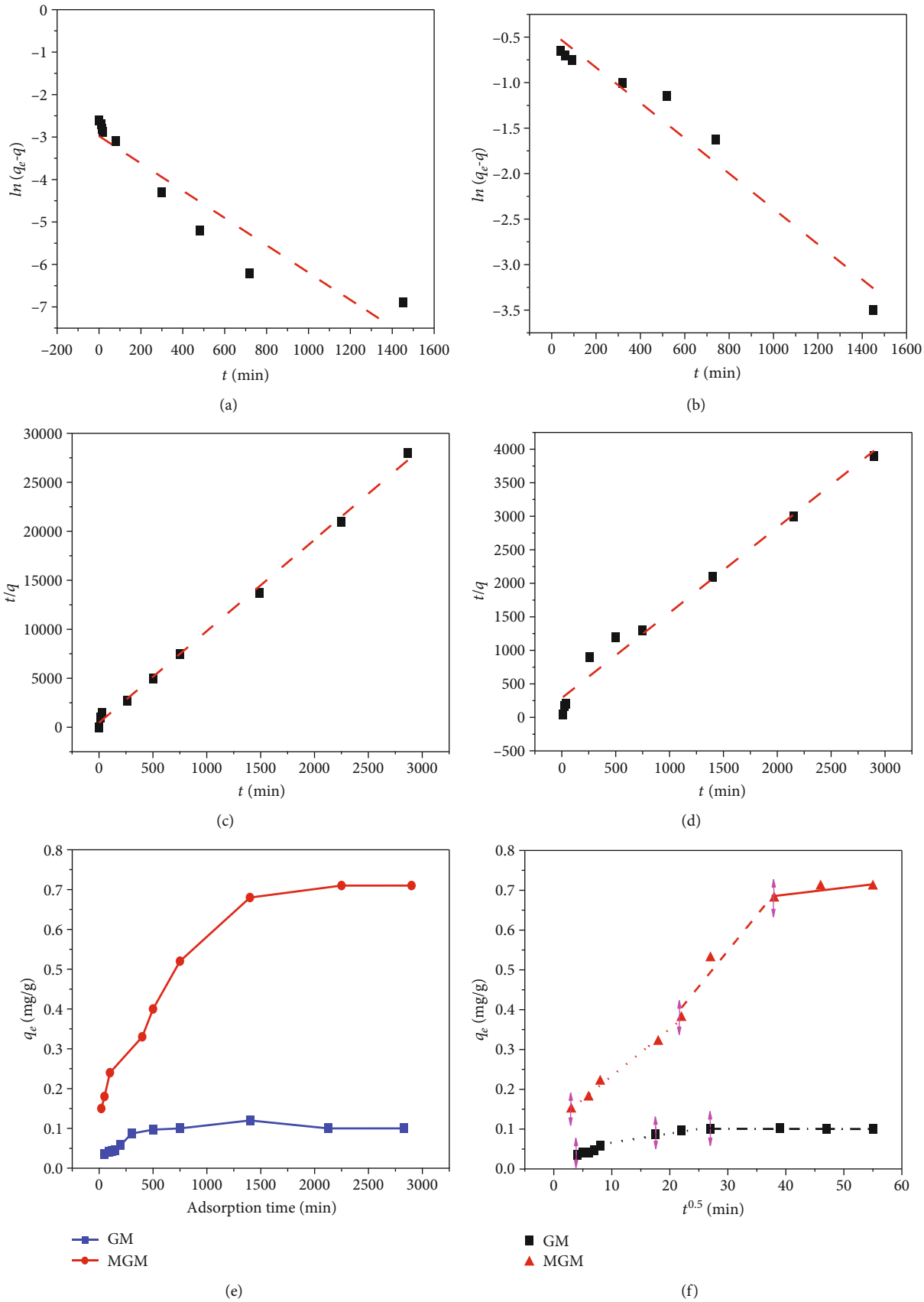

Figure 6: (a) Pseudo-first-order kinetic model for GM. (b) Pseudo-first-order kinetic model for MGM. (c) Pseudo-second-order model for GM. (d) Pseudo-second-order model for MGM. (e) The kinetic curves of GM and MGM. (f) Particle internal diffusion model of GM and MGM.

Table 2: Dynamic-related parameter values of phosphate adsorption by GM and MGM.

Sample	GM				MGM			
First-order kinetics	k_1		R_{1^2}		k_1		R_{1^2}	
	0.005		0.983		-0.003		0.930	
Second-order kinetics	k_2		R_{2^2}		k_2		R_{2^2}	
	0.269		0.999		0.020		0.999	
Particle internal diffusion model	k_{d1}	R_{1^2}	k_{d2}	R_{2^2}	k_{d1}	R_{1^2}	k_{d2}	R_{2^2}
	0.0039	0.974	0.00125	0.90612	0.01183	0.99392	0.01791	0.95522

Table 3: Langmuir, Freundlich, and Temkin adsorption constants and correlation coefficients of GM.

T	Constants	Langmuir	Constants	Freundlich	Constants	Temkin
293 K	q_m	0.191	K_F	0.079	A	0.096
	K_L	1.07	$1/n$	0.406	B	0.031
	R^2	0.932	R^2	0.968	R^2	0.889
303 K	q_m	0.173	K_F	0.080	A	0.097
	K_L	1.48	$1/n$	0.395	B	0.030
	R^2	0.914	R^2	0.951	R^2	0.894

Table 4: Langmuir, Freundlich, and Temkin adsorption constants and correlation coefficients of MGM.

T	Constants	Langmuir	Constants	Freundlich	Constants	Temkin
293 K	q_m	0.841	K_F	0.361	A	0.330
	K_L	0.421	$1/n$	0.254	B	0.143
	R^2	0.997	R^2	0.786	R^2	0.867
303 K	q_m	0.935	K_F	0.585	A	0.516
	K_L	1.053	$1/n$	0.150	B	0.135
	R^2	0.999	R^2	0.814	R^2	0.789

uneven surfaces with different adsorption energies, indicating that the surface of GM was uneven, and the adsorption process was multilayered. It could be seen from Table 4 that the fitting effect of the Langmuir equation of the MGM was obviously better than Freundlich and Temkin, which indicated that the adsorption process of the MGM changed from the original heterogeneous surface to the homogeneous surface, and multilayer adsorption changed to the single-layer adsorption [39].

It could be seen from Figure 7 that the adsorption capacity of GM and MGM increased with the increase of phosphate solution concentration. The difference was that the maximum adsorption capacity of GM and MGM increased from 0.183 mg/g to 0.78 mg/g and 0.191 mg/g to 0.90 mg/g at different temperatures, and the difference in the adsorption capacity between GM and MGM increased with the increasing initial phosphate concentration, indicating that the affinity of MGM to phosphate was higher than that of GM. It could also be seen from Figure 7 that the adsorption capacity of GM was not greatly affected by temperature, while the adsorption capacity of MGM was greatly affected by temperature and increased with the increase of temperature. This was because the adsorption process of GM was multilayer adsorption, and the adsorption process of MGM was single-layer adsorption. And with increasing in temperature, the diffusion of phosphate ions in the micropores of MGM increased, and more binding sites were occupied.

3.4. Adsorption Thermodynamics. Thermodynamic parameters depend on the reaction process. In order to further study the adsorption mechanism of MGM, the adsorption thermodynamics of MGM was studied. The results are shown in Table 5.

According to the thermodynamic data obtained in Table 5, $\Delta G < 0$ indicated that the adsorption process of MGM was spontaneous. In addition, the value of ΔG decreased with the increase of temperature, indicating that adsorption was a more favorable spontaneous reaction at high temperature. $\Delta H > 0$ indicated that there was an endothermic adsorption process in this process, which was consistent with the increase of adsorption capacity with the increase of temperature. With the increasing of temperature,

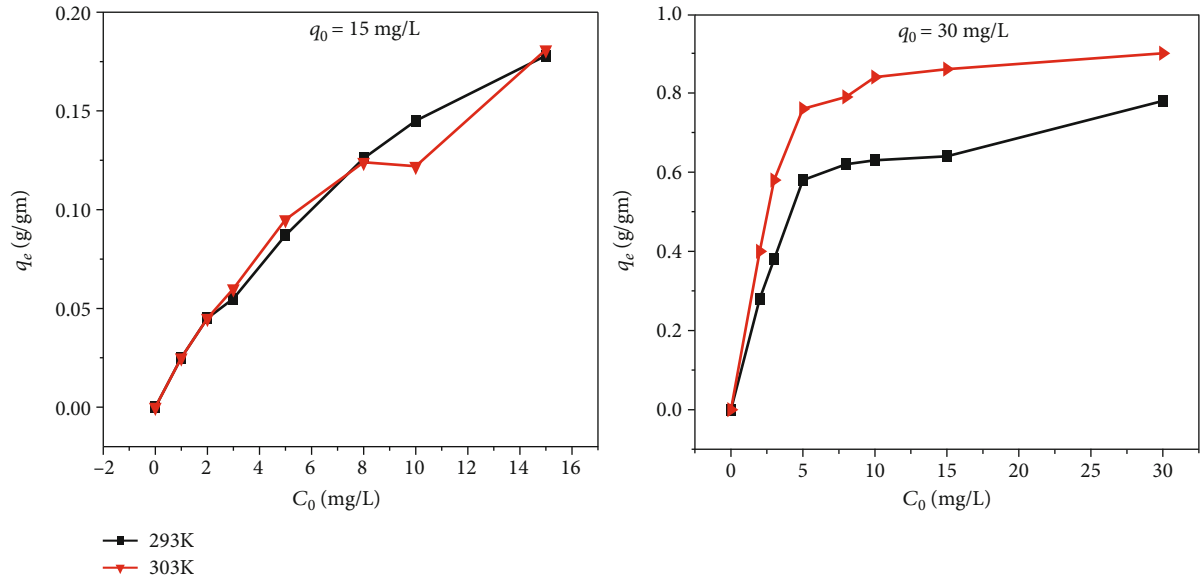

Figure 7: The phosphorus adsorption isotherm of GM and MGM.

Table 5: Thermodynamic parameters of phosphorus adsorption by MGM.

T/K	ΔH(kJ/mol)	ΔG(kJ/mol)	ΔS(J/mol/K)
293	21.1756	-2.48683	80.76
303		-3.29445	

the increase of adsorption capacity destroyed the influence of physical force on adsorption. At the same time, the increase of temperature was beneficial to the adsorption reaction through the activation of adsorption sites. $\Delta S > 0$, indicating that in the process of adsorption, the randomness of the interface between adsorbent and wastewater increased. The research trend of thermodynamics in this experiment was consistent with the adsorption trend of acid-modified kaolinite to chromium and iron ions [40].

3.5. Adsorption Stability Experiment

3.5.1. The pH Adaptability of Adsorbent. The pH of the solution had certain influence on the adsorption process, and pH affected the surface charge of adsorbent and molecular ionization degree of pollutants [41]. Under the conditions of temperature of 298 K, phosphate concentration of 5 mg/L, and pH of 5, 7, and 9, the influence of GM and MGM on the adsorption capacity is shown in Figure 8.

It could be seen from Figure 8 that with the increase of pH from 3 to 9, the adsorption amount of phosphorus of GM and MGM decreased, and this trend was similar to that of other adsorbents used for dephosphorization [42]. It could be seen that the adsorption effect of GM and MGM under acidic conditions was better than that under alkaline conditions.

First of all, different pH values corresponded to different anionic forms of phosphate. With the increase in the pH

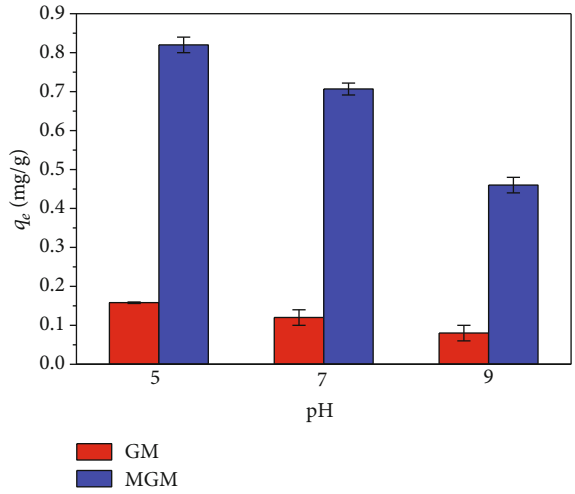

Figure 8: Adsorption effect on phosphorus under different pH values.

value of the solution, the phosphate changed from $H_2PO_4^-$ to HPO_4^-, and HPO_4^- was less conducive to adsorption than $H_2PO_4^-$. Therefore, the increase of pH inhibited the adsorption of phosphate on GM [43]; secondly, the electrostatic interaction between phosphate and GM also affected its adsorption of phosphate. When the pH value was lower than pH_{PZC}, the surfaces of GM and MGM were positively charged by protonation of their hydroxyl group, and the electrostatic force between the phosphate anion and the positively charged surface of GM and MGM was favorable for the adsorption of a phosphate anion. With an increase of the pH value beyond pH_{PZC}, the positive charge on the surface of GM decreased, thus weakening the electrostatic attraction. When the pH value was higher than pH_{PZC}, the surface of the GM was negatively charged by the deprotonation of its hydroxyl group. And as the pH value of the

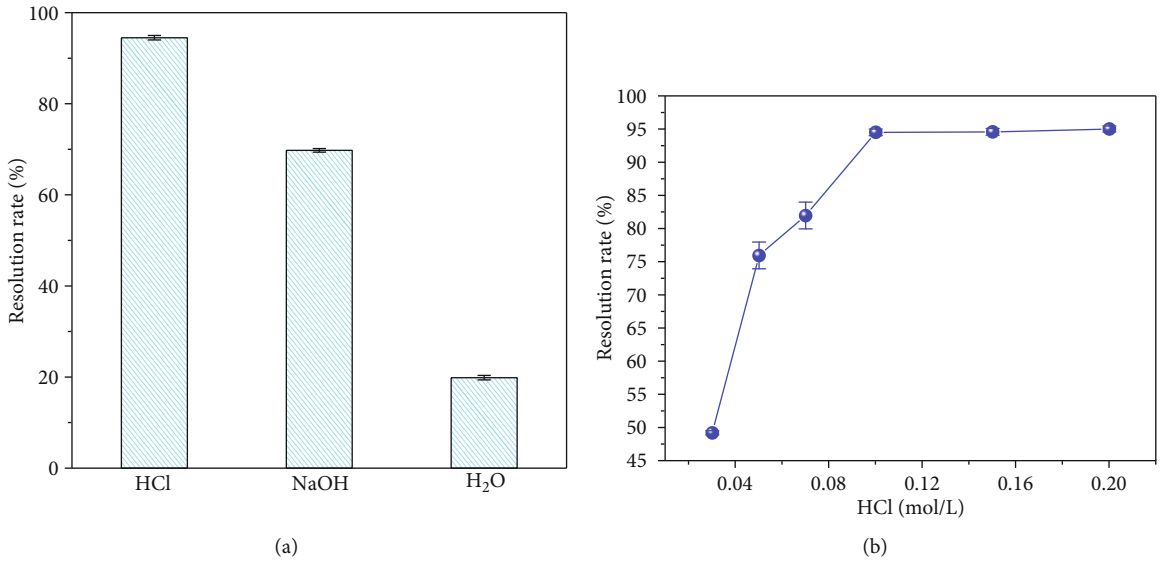

Figure 9: (a) Resolution rate of hydrochloric acid and sodium hydroxide. (b) Resolution rates of hydrochloric acid of different concentrations.

solution increased to 9, the surface charge of GM became more negative, so the electrostatic repulsion between the phosphate anion and the negatively charged GM surface increased, which reduced the amount of adsorbed phosphate [44]. Thirdly, the number of hydroxyl ions in the solution increased with the increase of the initial pH value of the solution, so the competition between hydroxyl ions and phosphate for adsorption active centers increased, resulting in the decrease of adsorption capacity [45]. In addition, it could be seen from Figure 8 that under different initial pH values, the phosphate content removed by the MGM was higher than that removed by the GM. The results showed that under different initial solution pH values, the adsorption of phosphate by MGM was higher than that of GM, and the adsorption effect of phosphate by MGM was good under acidic conditions. Therefore, this adsorbent also had some disadvantages such as a narrow pH range.

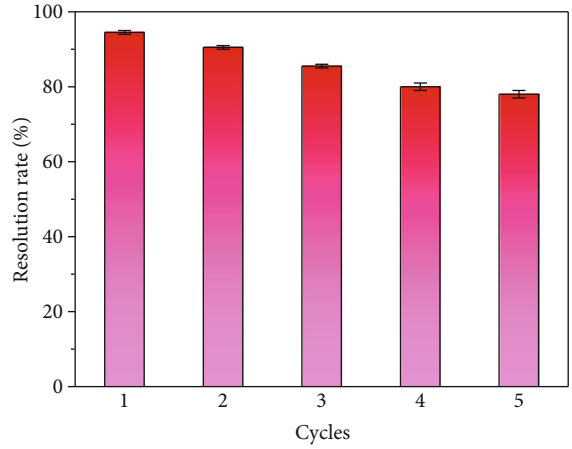

Figure 10: Resolution rate of MGM after multiple cycles.

3.5.2. Recycle Stability of Adsorbent

(1) Screening of Analytical Agents. The time of repeated use of the adsorbent was an important index to evaluate its adsorption capacity. Therefore, in order to investigate the recycling capacity of MGM, the MGM after the adsorption experiment was analyzed. Studies have shown that sodium hydroxide could be used as a regenerant, and it was considered that the solution with a lower pH value also has a certain research value [46]. Therefore, before medium regeneration, the analytical effect of 0.1 mol/L of hydrochloric acid and sodium hydroxide as the analytical agent is shown in Figure 9(a).

According to Figure 9(a), the resolution rate of hydrochloric acid was 94.5%, that of sodium hydroxide was 69.7%, and that of deionized water was 19.8%, and hydrochloric acid was clearly superior to sodium hydroxide. Therefore, hydrochloric acid was used as the phosphorus-resolving agent of MGM in this experiment.

(2) Effect of Hydrochloric Acid Concentration on Resolution. Based on the principle of economy and high efficiency, the analytical treatment results of saturated phosphorus MGM with hydrochloric acid concentrations of 0.03, 0.05, 0.07, 0.10, 0.15, and 0.2 mol/L are shown in Figure 9(b).

As could be seen from Figure 9(b), the concentration of hydrochloric acid increased from 0.03 mol/L to 0.10 mol/L, and the resolution rate increased from 49.4% to 94.5%, which greatly improved the resolution rate in this concentration range. However, when the concentration of hydrochloric acid was 0.15 mol/L, the resolution rate was 94.7%, and when the concentration was 0.20 mol/L, the resolution rate was 95.1%. It could be seen that the resolution rate increased little with the increase in concentration after the concentration was higher than 0.10 mol/L, so the optimal concentration was 0.10 mol/L.

Table 6: Comparison of phosphorus adsorbents.

Category	q_e (mg/g)	C_0 (mg/L)	pH	Reference
MGM	0.71 (298 K)	1-5	7	This study
MGM	0.78 (293 K)	0-30	7	This study
MGM	0.90 (303 K)	0-30	7	This study
GM	0.1 (298 K)	1-15	7	This study
Hematite	0.064 (293 K)	0-15	6.5	[48]
Kaolinite	0.491 (293 K)	0-15	6.5	[48]
Montmorillonite	0.228 (293 K)	0-15	6.5	[48]
Bentonite	0.24 (298 K)	0-300	7	[49]
Bauxite	0.61 (294 K)	2.5-40	5.9	[50]

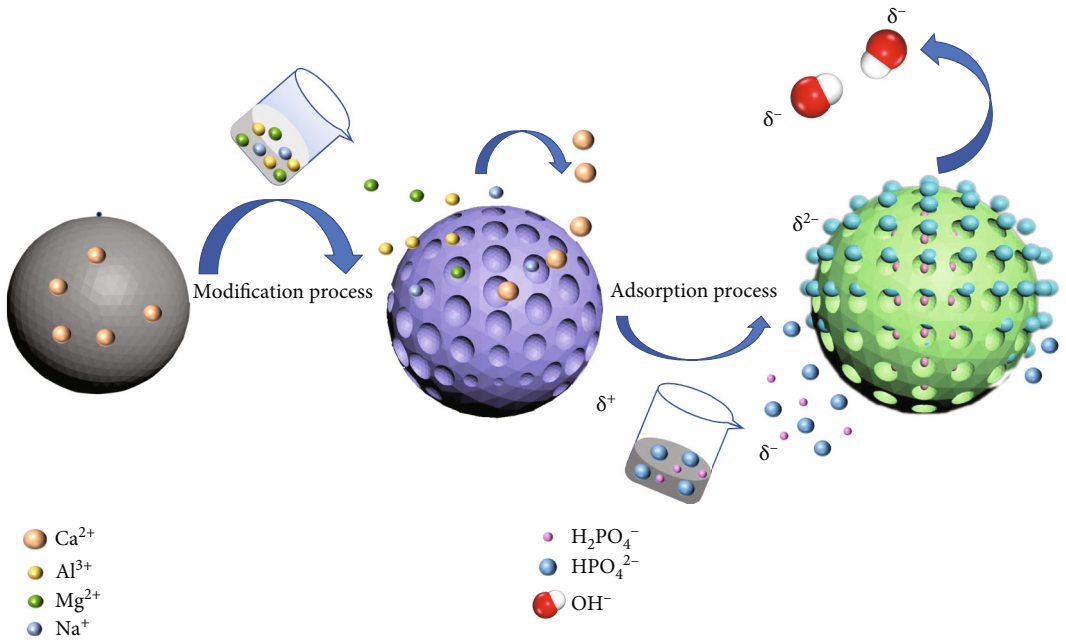

Figure 11: Adsorption mechanism.

(3) Analytical Effect of MGM. In order to evaluate the regeneration (analysis) potential of the medium, the analysis effect of MGM was studied, and the results are shown in Figure 10. It could be seen from Figure 10 that even after three regeneration cycles, a large amount of phosphorus was still removed from the tailings. The resolution rate of fresh MGM was 94.5%, and with the increase in circulation time, the resolution rate of MGM slowly decreased. After the third cycle, the resolution rate was around 85%. After five cycles, the resolution rate was still close to 80%. Therefore, the MGM was a stable and good phosphorus adsorbent. In order to further explore the practicability of MGM, the following research work can refer to the economic model proposed in [47] to analyze the relevant mechanism.

3.6. Analysis of Adsorption Performance and Mechanism of Adsorbent

3.6.1. Analysis of Adsorption Performance and Mechanism of Adsorbent. In this study, the phosphate adsorption capacities of GM, MGM, and other commonly used materials were compared, as shown in Table 6.

As can be seen from Table 6, MGM can be considered as a promising phosphorus removal material. The adsorption capacity of GM for phosphate is equivalent to other adsorbents and even lower than some adsorbents. The quality of phosphate adsorbed by MGM is 11 times higher than that of hematite, 2 times higher than that of kaolinite, and 3 times higher than that of bentonite and montmorillonite, which is equivalent to bauxite.

GM belonged to mine waste, and the rest belongs to mineral raw materials. GM was rich in montmorillonite, calcite, potash feldspar, and other minerals. Moreover, the adsorption of phosphate by GM has not been reported, and the adsorption of phosphate by MGM has also increased to a certain extent. Therefore, MGM had a good application prospect as a phosphate adsorbent, and it could better realize the goal of making waste from waste.

3.6.2. Adsorption Mechanism. According to the above research results and the previous research on mechanism

[51], the adsorption mechanism of phosphate by MGM could be obtained, as shown in Figure 11. Compared with GM, MGM had better phosphate adsorption capacity, which was due to the change of adsorbent surface properties. The adsorption mechanism of phosphate on MGM at initial pH 7 was studied. The adsorption and removal of most pollutants are not limited to physical adsorption or chemical adsorption; they can occur simultaneously and complement each other [52]. When the initial pH value was 7, it could be seen from the reaction equation (9) that there were high concentrations of $H_2PO_4^-$ and HPO_4^{2-}. The first driving force of phosphate adsorption was that the electrostatic interaction between negatively charged phosphate and positively charged adsorbent surface promoted the adsorption of phosphate on GM and MGM. This driving force is consistent with the research mechanism of methylene blue adsorption by a new adsorbent [53]. Another driving force of phosphate adsorption was that the ligand exchange between phosphate and hydroxyl was adsorbed on MGM, and OH^- was released in this process. Therefore, compared with unmodified GM, all these driving forces contribute to better adsorption of phosphate on MGM.

$$\begin{aligned} H_3PO_4 &\longrightarrow H_2PO_4^- + H^+ pK_{a1} = 2.16, \\ H_3PO_4 &\longrightarrow HPO_4^{2-} + H^+ pK_{a2} = 7.20, \\ H_3PO_4 &\longrightarrow PO_4^{3-} + H^+ pK_{a3} = 10.3. \end{aligned} \tag{9}$$

4. Conclusion

In this experiment, the removal effect of phosphorus from wastewater by GM and MGM was studied. Compared with GM, MGM had a rougher surface, larger pore size, higher specific surface area, and larger pore volume, thus improving adsorption performance. The adsorption kinetics of GM and MGM accorded with the quasi-second-order kinetic model. Before modification, it accorded with the Freundlich adsorption model, while the MGM accorded with the Langmuir equation. The internal diffusion model showed that the whole adsorption process of MGM was 700 min later than that before modification. Thermodynamic data showed that the increase of temperature was beneficial to the adsorption of MGM. With increasing pH from 3 to 9, the amount of phosphorus adsorption decreases GM and MGM, and the adsorption of phosphate by MGM was higher than that of GM. The phosphate adsorption effect of MGM in acidic condition was better than that in alkaline condition, so this adsorbent also has some shortcomings such as narrow pH range. Based on the principle of economy and high efficiency, hydrochloric acid with a concentration of 0.10 mol/L was used for analysis in this experiment. The results showed that the MGM had the highest resolution rate for phosphorus, and the resolution rate was still close to 80% after five cycles. Therefore, under the same conditions, the MGM had a higher phosphorus removal ability.

Data Availability

The data used to support the findings of this study are included within the article.

Conflicts of Interest

The authors declare that they have no known competing financial interests or personal relationships that could have appeared to influence the work reported in this paper.

Acknowledgments

This study was supported by the Liaoning Doctoral Research Start-up Fund (No. 2019-BS-087) and the Fundamental Research Funds for the Central Universities (N2001014).

References

[1] M. Lurling and F. Van Oosterhout, "Controlling eutrophication by combined bloom precipitation and sediment phosphorus inactivation," *Water Research*, vol. 47, no. 17, pp. 6527–6537, 2013.

[2] S. S. Lin, S. L. Shen, A. N. Zhou, and H. M. Lyu, "Sustainable development and environmental restoration in Lake Erhai, China," *Journal of Cleaner Production*, vol. 258, article 120758, 2020.

[3] E. Bulut, M. Ozacar, and I. A. Sengil, "Equilibrium and kinetic data and process design for adsorption of Congo Red onto bentonite," *Journal of Hazardous Materials*, vol. 154, no. 1-3, pp. 613–622, 2008.

[4] L. J. Wang, G. Pan, W. Q. Shi, Z. B. Wang, and H. G. Zhang, "Manipulating nutrient limitation using modified local soils: a case study at Lake Taihu (China)," *Water Research*, vol. 101, pp. 25–35, 2016.

[5] J. Marousek, L. Kolar, O. Strunecky et al., "Modified biochars present an economic challenge to phosphate management in wastewater treatment plants," *Journal of Cleaner Production*, vol. 272, article 123015, 2020.

[6] W. C. Lucas and M. Greenway, "Phosphorus retention by bioretention mesocosms using media formulated for phosphorus sorption: response to accelerated loads," *Journal of Irrigation and Drainage Engineering*, vol. 137, no. 3, pp. 144–153, 2011.

[7] T. Cai, S. Y. Park, and Y. B. Li, "Nutrient recovery from wastewater streams by microalgae: status and prospects," *Renewable & Sustainable Energy Reviews*, vol. 19, pp. 360–369, 2013.

[8] R. X. Hao, Y. Q. Zhou, J. B. Li, and J. C. Wang, "A 3DBER-S-EC process for simultaneous nitrogen and phosphorus removal from wastewater with low organic carbon content," *Journal of Environmental Management*, vol. 209, pp. 57–64, 2018.

[9] C. C. Zhou, G. J. Liu, S. C. Wu, and P. K. S. Lam, "The environmental characteristics of usage of coal gangue in bricking-making: a case study at Huainan, China," *Chemosphere*, vol. 95, pp. 274–280, 2014.

[10] J. Jang and D. S. Lee, "Effective phosphorus removal using chitosan/Ca-organically modified montmorillonite beads in batch and fixed-bed column studies," *Journal of Hazardous Materials*, vol. 375, pp. 9–18, 2019.

[11] D. Munkhbat, T. Ganbold, A. Naranbaatar, K. Shiomori, and O. Bayanjargal, "Pb(II) adsorption of composite alginate beads containing mesoporous natural zeolite," *Journal of Nanoscience and Nanotechnology*, vol. 20, no. 8, pp. 5267–5275, 2020.

[12] D. W. De Haas, M. C. Wentzel, and G. A. Ekama, "The use of simultaneous chemical precipitation in modified activated sludge systems exhibiting biological excess phosphate removal

part 1: literature review," *Water SA*, vol. 26, no. 4, pp. 439–452, 2000.

[13] J. Lalley, C. Han, X. Li, D. D. Dionysiou, and M. N. Nadagouda, "Phosphate adsorption using modified iron oxide-based sorbents in lake water: kinetics, equilibrium, and column tests," *Chemical Engineering Journal*, vol. 284, pp. 1386–1396, 2016.

[14] T. Panswad, A. Doungchai, and J. Anotai, "Temperature effect on microbial community of enhanced biological phosphorus removal system," *Water Research*, vol. 37, no. 2, pp. 409–415, 2003.

[15] Y. X. Qian, Y. H. Yuan, H. L. Wang et al., "Highly efficient uranium adsorption by salicylaldoxime/polydopamine graphene oxide nanocomposites," *Journal of Materials Chemistry A*, vol. 6, no. 48, pp. 24676–24685, 2018.

[16] C. Vohla, M. Koiv, H. J. Bavor, F. Chazarenc, and U. Mander, "Filter materials for phosphorus removal from wastewater in treatment wetlands–a review," *Ecological Engineering*, vol. 37, no. 1, pp. 70–89, 2011.

[17] H. Y. Jin, L. Lin, X. Y. Meng et al., "A novel lanthanum-modified copper tailings adsorbent for phosphate removal from water," *Chemosphere*, vol. 281, article 130779, 2021.

[18] L. Johansson and J. P. Gustafsson, "Phosphate removal using blast furnace slags and opoka-mechanisms," *Water Research*, vol. 34, no. 1, pp. 259–265, 2000.

[19] R. Saad, S. Hamoudi, and K. Belkacemi, "Adsorption of phosphate and nitrate anions on ammonium-functionnalized mesoporous silicas," *Journal of Porous Materials*, vol. 15, no. 3, pp. 315–323, 2008.

[20] R. Zhou, Y. Wang, M. Zhang, P. X. Yu, and J. Li, "Adsorptive removal of phosphate from aqueous solutions by thermally modified copper tailings," *Environmental Monitoring and Assessment*, vol. 191, no. 4, p. 198, 2019.

[21] P. Wang, F. Ding, Z. Huang, Z. Fu, P. Zhao, and S. Men, "Adsorption behavior and mechanism of Cd (II) by modified coal-based humin," *Environmental Technology & Innovation*, vol. 23, article 101699, 2021.

[22] R. Mudzielwana, M. W. Gitari, and P. Ndungu, "Performance evaluation of surfactant modified kaolin clay in As(III) and As(V) adsorption from groundwater: adsorption kinetics, isotherms and thermodynamics," *Heliyon*, vol. 5, no. 11, article e02756, 2019.

[23] E. Krawczyk-Bärsch, T. Arnold, H. Reuther, F. Brandt, D. Bosbach, and G. Bernhard, "Formation of secondary Fe-oxyhydroxide phases during the dissolution of chlorite - effects on uranium sorption," *Applied Geochemistry*, vol. 19, no. 9, pp. 1403–1412, 2004.

[24] S. Bhattacharya, N. Bar, B. Rajbansi, and S. K. Das, "Adsorptive elimination of Cu(II) from aqueous solution by chitosan-nanoSiO2 nanocomposite—adsorption study, MLR, and GA modeling," *Water, Air, & Soil Pollution*, vol. 232, no. 4, 2021.

[25] J. H. Qiu, X. S. Du, S. Komarneni, H. B. Wang, X. Cheng, and Z. L. Du, "Preparation of polyacrylamide–montmorillonite nanocomposite and its application in Cr(III) adsorption," *Journal of Applied Polymer Science*, vol. 137, no. 36, article 49065, 2020.

[26] L. R. Somera, R. Cuazon, J. K. Cruz, and L. J. Diaz, "Kinetics and isotherms studies of the adsorption of Hg(II) onto iron modified montmorillonite/polycaprolactone nanofiber membrane," in *2019 2nd International Conference on Materials Engineering and Applications (Icmea 2019)*, vol. 540, Da Nang, Vietnam, 2019.

[27] S. Hussain, H. A. Aziz, M. H. Isa et al., "Orthophosphate removal from domestic wastewater using limestone and granular activated carbon," *Desalination*, vol. 271, no. 1-3, pp. 265–272, 2011.

[28] N. Y. Mezenner and A. Bensmaili, "Kinetics and thermodynamic study of phosphate adsorption on iron hydroxide- eggshell waste," *Chemical Engineering Journal*, vol. 147, no. 2-3, pp. 87–96, 2009.

[29] J. A. Rentz, I. P. Turner, and J. L. Ullman, "Removal of phosphorus from solution using biogenic iron oxides," *Water Research*, vol. 43, no. 7, pp. 2029–2035, 2009.

[30] S. Sarkar, N. Tiwari, M. Behera et al., "Facile synthesis, characterization and application of magnetic Fe_3O_4-coir pith composites for the removal of methyl violet from aqueous solution: kinetics, isotherm, thermodynamics and parametric optimization," *Journal of the Indian Chemical Society*, vol. 99, no. 5, article 100447, 2022.

[31] T. Ye, X. Min, X. Li, S. Zhang, and Y. Gao, "Improved holding and releasing capacities of coal gangue toward phosphate through alkali-activation," *Chemosphere*, vol. 287, Part 4, article 132382, 2022.

[32] Z. Guo, J. Zhang, Y. Kang, and H. Liu, "Rapid and efficient removal of Pb(II) from aqueous solutions using biomass-derived activated carbon with humic acid in-situ modification," *Ecotoxicology and Environmental Safety*, vol. 145, pp. 442–448, 2017.

[33] H. Fu, Y. Li, Z. Yu et al., "Ammonium removal using a calcined natural zeolite modified with sodium nitrate," *Journal of Hazardous Materials*, vol. 393, article 122481, 2020.

[34] H. U. So, D. Postma, R. Jakobsen, and F. Larsen, "Sorption of phosphate onto calcite; results from batch experiments and surface complexation modeling," *Geochimica et Cosmochimica Acta*, vol. 75, no. 10, pp. 2911–2923, 2011.

[35] A. Sari and M. Tuzen, "Adsorption of silver from aqueous solution onto raw vermiculite and manganese oxide-modified vermiculite," *Microporous and Mesoporous Materials*, vol. 170, pp. 155–163, 2013.

[36] H. Yang, Y. Sun, Q. Zhang et al., "$ZrMO_X$ particles for enhanced removal of methyl orange from wastewater: preparation, characterization, and adsorption study," *Adsorption Science & Technology*, vol. 2022, Article ID 9685352, 11 pages, 2022.

[37] K. W. Jung, M. J. Hwang, K. H. Ahn, and Y. S. Ok, "Kinetic study on phosphate removal from aqueous solution by biochar derived from peanut shell as renewable adsorptive media," *International journal of Environmental Science and Technology*, vol. 12, no. 10, pp. 3363–3372, 2015.

[38] M. Uçar, "Adsorption of chlorophenolic compounds on activated clinoptilolite," *Adsorption Science & Technology*, vol. 37, no. 7-8, pp. 664–679, 2019.

[39] X. C. Wei, R. C. Viadero, and S. Bhojappa, "Phosphorus removal by acid mine drainage sludge from secondary effluents of municipal wastewater treatment plants," *Water Research*, vol. 42, no. 13, pp. 3275–3284, 2008.

[40] P. E. Dim, L. S. Mustapha, M. Termtanun, and J. O. Okafor, "Adsorption of chromium (VI) and iron (III) ions onto acid-modified kaolinite: Isotherm, kinetics and thermodynamics studies," *Arabian Journal of Chemistry*, vol. 14, no. 4, article 103064, 2021.

[41] D. Luo, L. Y. Wang, H. Y. Nan et al., "Phosphorus adsorption by functionalized biochar: a review," *Environmental Chemistry Letters*, vol. 21, no. 1, pp. 497–524, 2023.

[42] D. W. Schindler, R. E. Hecky, D. L. Findlay et al., "Eutrophication of lakes cannot be controlled by reducing nitrogen input: results of a 37-year whole-ecosystem experiment," *Proceedings of the National Academy of Sciences of the United States of America*, vol. 105, no. 32, pp. 11254–11258, 2008.

[43] Q. Z. Xu and B. R. Huang, "Effects of differential air and soil temperature on carbohydrate metabolism in creeping bentgrass," *Crop Science*, vol. 40, no. 5, pp. 1368–1374, 2000.

[44] K. H. Goh, T. T. Lim, and Z. Dong, "Application of layered double hydroxides for removal of oxyanions: a review," *Water Research*, vol. 42, no. 6-7, pp. 1343–1368, 2008.

[45] C. Barca, C. Gerente, D. Meyer, F. Cliazarenc, and Y. Andres, "Phosphate removal from synthetic and real wastewater using steel slags produced in Europe," *Water Research*, vol. 46, no. 7, pp. 2376–2384, 2012.

[46] T. V. Sima, M. W. Letshwenyo, and L. Lebogang, "Efficiency of waste clinker ash and iron oxide tailings for phosphorus removal from tertiary wastewater: batch studies," *Environmental Technology & Innovation*, vol. 11, pp. 49–63, 2018.

[47] A. Das, N. Bar, and S. K. Das, "Adsorptive removal of Pb (II) ion on *Arachis hypogaea*'s shell: batch experiments, statistical, and GA modeling," *International journal of Environmental Science and Technology*, vol. 20, no. 1, pp. 537–550, 2023.

[48] H. Fang, Z. Cui, G. He, L. Huang, and M. Chen, "Phosphorus adsorption onto clay minerals and iron oxide with consideration of heterogeneous particle morphology," *Science of the Total Environment*, vol. 605-606, pp. 357–367, 2017.

[49] X. Chen, L. Wu, F. Liu et al., "Performance and mechanisms of thermally treated bentonite for enhanced phosphate removal from wastewater," *Environmental Science and Pollution Research International*, vol. 25, no. 16, pp. 15980–15989, 2018.

[50] A. Drizo, C. A. Frost, J. Grace, and K. A. Smith, "Physico-chemical screening of phosphate-removing substrates for use in constructed wetland systems," *Water Research*, vol. 33, no. 17, pp. 3595–3602, 1999.

[51] C. Wang, R. Sun, and R. Huang, "Highly dispersed iron-doped biochar derived from sawdust for Fenton-like degradation of toxic dyes," *Journal of Cleaner Production*, vol. 297, article 126681, 2021.

[52] Z. Kang, X. Jia, Y. Zhang et al., "A review on application of biochar in the removal of pharmaceutical pollutants through adsorption and persulfate-based AOPs," *Sustainability*, vol. 14, no. 16, article 10128, 2022.

[53] J. Bu, L. Yuan, H. Jiang, and C. Wang, "Study on removal of methylene blue by condensation self-assembled graphene oxide/Thiourea composite adsorbent," *Sustainability*, vol. 14, no. 22, article 15290, 2022.